Cooperative biexciton generation and destructive interference in coupled quantum dots using adiabatic rapid passage

Nicolas Renaud* and Ferdinand C. Grozema†
Opto-Electronic Materials Section, Department of Chemical Engineering, Delft University of Technology, Julianalaan 136, 2629BL, Delft, The Netherlands
(Received 27 June 2014; revised manuscript received 18 September 2014; published 22 October 2014)

We report numerical simulations of biexciton generation in coupled quantum dots (CQDs) placed in a static electric field and excited by a chirped laser pulse. Our simulations explicitly account for exciton-phonon interactions at finite temperature using a non-Markovian quantum jump approach to solve the excitonic dynamics. In the case of noninteracting quantum dots, the biexciton generation is severely limited by the biexciton binding energy. We demonstrate that the application of an axial electric field along the CQDs can yield a favorable excitonic level alignment that compensates for the biexciton binding energy and yields an optimum biexciton generation. On the contrary, well-defined values of the electric field lead to destructive quantum interference that completely inhibits the biexciton generation. We therefore demonstrate here the potential of chirped pulse excitations of CQDs for high-efficiency biexciton generation but also for the control of unique optoelectronic properties of complex quantum systems.

DOI: 10.1103/PhysRevB.90.165307 PACS number(s): 03.65.Yz, 78.67.Hc, 42.50.Ct, 63.20.kk

I. INTRODUCTION

The robust generation of high-quality biexcitons in semiconductor quantum dots (QDs) is of prime importance for the development of quantum information as their radiative decay can be used as a source of entangled photon pairs [1,2]. An ideal biexciton generation can in principle be achieved using Rabi oscillations [3–5]. However, the final biexciton population obtained via this simple scheme depends strongly on the intensity and duration of the laser pulse and is therefore not robust against experimental parameters. To overcome this difficulty, it has recently been proposed to use adiabatic rapid passage (ARP) techniques [6] to obtain a robust control of the final exciton [7–12] or biexciton [13–16] population of isolated QDs at finite temperature.

These studies have, however, shown that the efficiency of biexciton generation is severely limited by the biexciton binding energy [14,16], noted δ in the following, which can range between a few and a few tens of meV, depending on the nature and size of the QD [17–19]. Due to the binding energy of the biexciton, the central frequency of the laser pulse, usually set at half the biexciton energy, is off-resonant with the transition to the first excited state of the QD. As a consequence of this detuning, intense laser pulses are needed to obtain a significant population of the biexcitonic state even for a biexciton binding energy of only a few meV [14]. Several solutions have been devised to circumvent this issue. It is possible, for example, to benefit from phonon-induced dephasing [16] or to use a two-color ARP scheme [14] to compensate for the effect of δ. However, these elegant solutions come with inherent experimental complications, such as the necessity to use two distinct frequency swept laser pulses [14].

While the chirped pulse excitation of isolated QDs have been intensively studied, little is known about the efficiency of such process for coupled quantum dots (CQDs) [20,21]. The energy levels and mutual electronic and excitonic couplings between the dots can be finely tuned by engineering their structure and by carefully controlling the interdot distance [22–25]. The possibility to apply an electric field along the dimer [26,27] using an external gate voltage adds a supplementary means to control these energy levels [28–31]. Such electronic structure manipulation by an external field has already been employed to generate well-defined entangled states [32,33] or for the realization of conditional logic [34] using CQDs.

In this paper, we study the biexciton generation in CQDs placed in a static electric field and excited by a chirped laser pulse. Different theoretical approaches have been developed to account for exciton-phonon (ex-ph) interactions during the ARP excitation of isolated QDs [35–37]. Most of these approaches are based on the propagation of the density matrix of the system under consideration using the Born-Markov approximation [9] or correlation expansion techniques [14]. The computational cost of these techniques scales quadratically with the system size, which might be prohibitive to study large quantum systems. In the work presented here, the simulation of the excitonic dynamics is performed using the recently developed non-Markovian quantum jump (NMQJ) approach [38] combined with a Chebyshev expansion of the evolution operator [39].

The NMQJ approach is based on a non-Hermitian deterministic propagation of the wave function interrupted by stochastic quantum jumps [40,41]. Consequently the NMQJ does not require the propagation of the density matrix of the system and might therefore be more appropriate than Liouville-space approaches to study the dynamics of large open quantum systems. However, its computational efficiency should be similar to density matrix propagation techniques for small systems due to the extra numerical effort required to perform the quantum jumps. In contrast with many density matrix propagation techniques [9], the NMQJ approach avoids the Markov approximation [41,42]. As a consequence, the time-dependent relaxation rates used in the NMQJ approach depend not only on the instantaneous energies of the system,

*n.renaud@tudelft.nl
†f.grozema.tudelft.nl

but also on their entire evolution from the starting point of the dynamics [42]. The NMQJ is, however, an intrinsically numerical approach and is therefore unable to provide on its own analytic solutions such as the ones developed in Ref. [13]. It has, however, been shown that the NMQJ approach converges to the exact solution of the master equation in selected cases [41]. Besides, unlike real-time path-integral approaches [43], the NMQJ cannot account for an arbitrary multiphonon process as only the second-order exciton-phonon interaction terms are kept in the master equation. Despite the significant differences outlined above, these different techniques should, however, lead to comparable results for the systems studied in this paper.

In this paper, we first study the case of an isolated QD to validate our numerical approach. In agreement with previous studies [14], we observe a significant degradation of the biexciton generation with the biexciton binding energy. We then consider the case of CQDs placed in a static external electric field and excited with a chirped laser pulse. Our results demonstrate that favorable values for the electric field lead to a significant improvement of the biexciton generation even for large values of the biexciton binding energy and low intensities of the laser pulse. On the contrary, well-defined values of the electric field lead to destructive quantum interference and totally inhibit the biexciton generation. The excitation of CQDs with chirped laser pulses not only provides an attractive route for efficient biexciton generation, but it also offers an ideal platform to probe the unique optoelectronic properties of complex quantum systems.

II. NON-MARKOVIAN QUANTUM JUMP FOR AN EXPLICITLY TIME-DEPENDENT HAMILTONIAN

The Hamiltonian of a QD system in interaction with a laser pulse and in the presence of exciton-phonon coupling can be written as $\mathcal{H} = \mathcal{H}_0 + \mathcal{H}_{\mathcal{E}}(t) + \mathcal{H}_B + \mathcal{H}_{SB}$, where $\mathcal{H}_0$ is the Hamiltonian of the isolated QD, $\mathcal{H}_{\mathcal{E}}(t)$ is the interaction Hamiltonian between the QDs and the incident laser field, $\mathcal{H}_B$ is the Hamiltonian of the bath, formed here by the phonon modes of the QDs, and $\mathcal{H}_{SB}$ the ex-ph interaction Hamiltonian. In the local basis set, i.e., in the basis formed by the excitations of each QD, $\mathcal{H}_0$ reads

$$\mathcal{H}_0 = \sum_{n=1}^{N_S} \epsilon_n |n\rangle\langle n| + \sum_{m<n}^{N_S} V_{nm}(|n\rangle\langle m| + |m\rangle\langle n|), \tag{1}$$

where N_S is the total number of states in the system, ϵ_n is the energy of the excited state $|n\rangle$, and V_{nm} is the electronic or excitonic coupling between the states $|n\rangle$ and $|m\rangle$. This Hamiltonian can equivalently be expressed in its diagonal basis set by $\mathcal{H}_0 = \sum_M E_M |M\rangle\langle M|$, where E_M is the energy of the Mth diagonal state and $|M\rangle = \sum_n m_n |n\rangle$ is the Mth diagonal state. The excitation of the QDs is operated by the Hamiltonian $\mathcal{H}_{\mathcal{E}}(t)$ that reads

$$\mathcal{H}_{\mathcal{E}}(t) = \sum_{n=1}^{N_S} \sum_{m<n}^{N_S} \frac{1}{2} \mu_{nm} \Omega(t)(|n\rangle\langle m| + |m\rangle\langle n|), \tag{2}$$

where μ_{nm} is the transition dipole moment between the states $|n\rangle$ and $|m\rangle$, and $\Omega(t)$ is the electric field. Adiabatic rapid passage is achieved using a linearly chirped Gaussian pulse [6]:

$$\Omega(t) = \frac{\Theta}{\sqrt{2\pi}\tau_0 \tau} \exp\left(-\frac{t^2}{\tau^2}\right) \exp(-i\omega_l t - iat^2), \tag{3}$$

where Θ is the pulse area, i.e., the square root of the pulse intensity, and ω_l is the central frequency of the laser pulse. Experimentally, such a pulse can be created by passing a transform-limited pulse through a Gaussian chirp filter that introduces a quadratic phase α. The chirp filter modifies the pulse length, which becomes $\tau = (\alpha^2/\tau_0^2 + \tau_0^2)^{1/2}$ and introduces a chirp rate $a = \alpha/(\alpha^2 + \tau_0^4)$ [11]. The Hamiltonian of the driven system is given by

$$\mathcal{H}_S = \mathcal{H}_0 + \mathcal{H}_{\mathcal{E}}(t). \tag{4}$$

The eigenstates of $\mathcal{H}_S$ are referred to as the dressed states and can be expressed in the local basis as

$$|\Psi_\alpha(t)\rangle = \sum_m c_{\alpha,m}(t)|m\rangle. \tag{5}$$

As demonstrated in previous publications [8,14], the time evolution of the dressed states is of key importance for the comprehension of the dephasing and energy relaxation observed during the ARP excitation of QDs.

In the following, we assume that the exciton-phonon interactions principally lead to fluctuations in the QD energy levels [42]. We consequently neglect any variations of the interdot couplings induced by the phonon modes of the crystal. Under this assumption, the exciton-phonon interaction Hamiltonian reads [42]

$$\mathcal{H}_{SB} = \sum_{n=1}^{N_S} \mathcal{S}_n \otimes \sum_q (g_q b_q + g_q^* b_q^\dagger). \tag{6}$$

In Eq. (6), the operators $\mathcal{S}_n$ are diagonal matrices defined by [42]

$$\mathcal{S}_n = \eta_n |n\rangle\langle n|, \tag{7}$$

where η_n is equal to the number of excitons in the local state $|n\rangle$ [14]. In Eq. (6), g_q is the interaction strength with the qth mode of the bath, and $b_q^\dagger$ (b_q) creates (destroys) a phonon in the qth mode. Finally, the phonon Hamiltonian is defined by [44]

$$\mathcal{H}_B = \sum_i \hbar\omega_i b_i^\dagger b_i. \tag{8}$$

Using the Hamiltonian described above, one can show that the second-order time-convolutionless master equation governing the dynamics can be written as [41,42,44]

$$\begin{aligned}\frac{d}{dt}\rho_S(t) = &-\frac{i}{\hbar}[\mathcal{H}_S(t), \rho_S(t)] \\ &+ \sum_{\alpha,\beta} \gamma_{\alpha\beta}(t) A_{\alpha\beta}(t) \rho_S(t) A_{\alpha\beta}^\dagger(t) \\ &- \frac{1}{2} \sum_{\alpha,\beta} \gamma_{\alpha\beta}(t) \{A_{\alpha\beta}^\dagger(t) A_{\alpha\beta}(t), \rho_S(t)\},\end{aligned} \tag{9}$$

where $\rho_S(t)$ is the reduced density matrix on the excitonic states, and where the operators

$$A_{\alpha\beta}(t) = s_{\alpha\beta}(t) |\Psi_\alpha(t)\rangle\langle\Psi_\beta(t)| \tag{10}$$

describe the exciton-phonon interactions [44]. A detailed derivation of this equation can be found in Ref. [42]. Based on the Born approximation, Eq. (9) is limited to weak system-bath interaction and does not account for multiphonon processes. In Eq. (10), the coefficients $s_{\alpha\beta}(t)$ come from the development of the operators $\mathcal{S}_n$, introduced in Eq. (6), on the time-dependent basis formed by the instantaneous dressed states [42]:

$$s_{\alpha\beta}(t) = \sum_{n=1}^{N_S} \eta_n c_{n,\alpha}(t) c^*_{n,\beta}(t). \tag{11}$$

Contrary to the Markovian limit, the decay rates, $\gamma_{\alpha\beta}(t)$, present in Eq. (9) are time-dependent here and can take positive and negative values. The time intervals where a given decay rate takes negative values are characteristic of non-Markovian memory effects [41]. For finite temperature, these decay rates can be expressed as [42]

$$\gamma_{\alpha\beta}(t) = \int_0^t d\tau \int_0^\infty d\nu\, \mathcal{J}(\nu) n(\nu) \cos\{[\omega_{\alpha\beta}(\tau) + \nu]\tau\} + \mathcal{J}(\nu)[n(\nu)+1]\cos\{[\omega_{\alpha\beta}(\tau) - \nu]\tau\}, \tag{12}$$

where $\mathcal{J}(\nu)$ is the spectral density of the bath modes, $n(\nu)$ is the bosonic distribution function, and $\omega_{\alpha\beta}(\tau)$ is the energy difference between the dressed states $|\Psi_\alpha(t)\rangle$ and $|\Psi_\beta(t)\rangle$. These energy differences here are explicitly time-dependent due to the interaction between the QDs and the laser field.

Following the NMQJ approach, the master equation (9) is solved following a statistical approach using an ensemble of N_{real} realizations of the system state vector. In the following, we use an ensemble size of $N_{\text{real}} = 10^5$. At any time of the simulation, the reduced density matrix, $\rho_S(t)$, can be obtained by averaging over the state vector ensemble [38]:

$$\rho_S(t) = \frac{N_0(t)}{N_{\text{real}}} |\Psi_0(t)\rangle\langle\Psi_0(t)| + \sum_{\alpha=1}^{N_S} \frac{N_\alpha(t)}{N_{\text{real}}} |\Psi_\alpha(t)\rangle\langle\Psi_\alpha(t)|. \tag{13}$$

In this equation, the state $|\Psi_0(t)\rangle$ is the propagated initial state of the dynamics [41]. Its initial weight in the ensemble is consequently $N_0(t=0) = N_{\text{real}}$. The remaining states in the ensemble, i.e., $|\Psi_\alpha(t)\rangle$ with $\alpha = 1, N$, correspond to the instantaneous dressed states. During each time step, Δt, of the dynamics, $|\Psi_0(t)\rangle$ evolves in a deterministic fashion and the weights $N_i(t)$ with $i = 0 - N_S$ are modified according to a well-defined conserving stochastic process [38].

The deterministic evolution of $|\Psi_0(t)\rangle$ is driven by a non-Hermitian Monte Carlo effective Hamiltonian [40]:

$$\mathcal{H}_{\text{eff}}(t) = \mathcal{H}_S(t) - i\frac{\hbar}{2}\sum_{\alpha,\beta} \gamma_{\alpha,\beta}(t) A^\dagger_{\alpha\beta}(t) A_{\alpha\beta}(t). \tag{14}$$

As a consequence of the explicit time dependence in $\mathcal{H}_{\text{eff}}(t)$, the first-order expansion of the evolution operator usually used in the NMQJ implementation [41,42] is not suitable here to propagate the wave function. Instead, the evolution operator is expanded in a Chebyshev series [39]:

$$|\Psi_0(t+\Delta t)\rangle = \left(\sum_{i=0}^{N_C} a_i \phi_i(-i\tilde{\mathcal{H}}_{\text{eff}}\Delta t)\right)|\Psi_0(t)\rangle, \tag{15}$$

where a_i are the expansion coefficients and ϕ_i are the complex Chebyshev polynomials defined by their recurrence relation [39]. A total of $N_C = 50$ polynomials were used in the expansion, and a time increment of $\Delta t = 10$ fs was set to solve the dynamics. The accuracy of the dynamics obtained with Eq. (15) was checked for selected cases using an iterative time-ordering Chebyshev (ITOC) expansion [45,46]. This highly accurate approach adds a supplementary iterative loop to the Chebyshev expansion (15) to account for the time-ordering operator [45]. As a consequence of this additional loop, the error propagated during the dynamics using the ITOC expansion can be brought to machine precision even for intense laser pulses and large time increments. No significant differences were observed between the dynamics obtained via these two numerical approaches. This confirms the adequacy of the Chebyshev expansion given in Eq. (15) to solve the dynamics of the systems studied here. Finally, let us mention that due to the diagonal non-Hermitian part in the Hamiltonian (14), a normalization of $|\Psi_0(t)\rangle$ is required at the end of each time step [40,41].

The stochastic process governing the evolution of the statistical weights $N_\alpha(t)$ during each time step depends on the values of the decay rates $\gamma_{\alpha\beta}(t)$ [38]. If $\gamma_{\alpha\beta}(t)$ is positive, the jump operator $A_{\alpha\beta}(t)$ can transfer ensemble members from any propagated state, $|\Psi_\kappa(t)\rangle$, to the target state of the jump operator: $|\Psi_\alpha(t)\rangle$. The probability of such a jump, referred to as a Markovian jump, is given by [41]

$$P_{\kappa,\alpha\beta}(t) = \gamma_{\alpha\beta}(t) p_{\kappa,\alpha\beta}(t)\Delta t \tag{16}$$

with $p_{\kappa,\alpha\beta}(t) = \langle\Psi_\kappa(t)|A^\dagger_{\alpha\beta}(t)A_{\alpha\beta}(t)|\Psi_\kappa(t)\rangle$. Therefore, the jump probability depends on the overlap $\langle\Psi_\kappa|\Psi_\beta\rangle$. This overlap is non-null only for $\kappa = \beta$ or for $\kappa, \beta = 0$ as $|\Psi_0(t)\rangle$ is a superposition of the N_S dressed states.

If the rate $\gamma_{\alpha\beta}(t)$ is negative, a so-called non-Markovian jump occurs and the direction of the jump is reversed [38]. Therefore, ensemble members that had previously been transferred to state $|\Psi_\alpha(t)\rangle$ by a Markovian jump can be transferred back to $|\Psi_\kappa(t)\rangle$ during a non-Markovian jump. The probability of such jump is given by [41]

$$\overline{P_{\kappa,\alpha\beta}}(t) = \frac{N_\kappa(t)}{N_\alpha(t)} |\gamma_{\alpha\beta}(t)| p_{\kappa,\alpha\beta}(t)\Delta t. \tag{17}$$

If during the time interval Δt, z ensemble members are transferred from $|\Psi_k(t)\rangle$ to $|\Psi_m(t)\rangle$ by a Markovian or non-Markovian jump, the statistical weights are modified according to $N^m_k(t+\Delta t) = N^m_k(t) \pm z$. Following the original MCWF approach, the number of transferred states is determined by a Monte Carlo process using the jump probability (16) or (17) for Markovian and non-Markovian jumps, respectively.

As clearly explained in Ref. [41], the master equation (9) does not ensure that the density matrix remains positive during the dynamics. This violation of the density matrix positivity occurs when $\gamma_{\alpha\beta}(t) < 0$ and simultaneously $N_\alpha(t) = 0$. The detection of such an event is straightforward, and nonphysical evolution can be easily identified. However, such a violation of the positivity of the density matrix was not observed for the set of parameters used in this paper.

III. BIEXCITON GENERATION IN ISOLATED QUANTUM DOTS

To validate the theoretical framework described above, we have calculated the biexciton generation obtained via ARP on a single QD. Recent articles have tackled this issue and underlined the impact of the biexciton binding energy on the final biexciton population [13,14]. In the following, we label the local excited states as $|^e_h X\rangle$, where e and h are the number of excited electrons and holes in the QD, respectively. The isolated QD studied here is consequently modeled by its ground state $|0\rangle$, its singly excited state $|^1_1 X\rangle$, and its biexcitonic state $|^2_2 X\rangle$. The energy of the single excitonic state is labeled $E_{|^1_1 X}$ and the energy of the biexcitonic state is given by

$$E_{|^2_2 X} = 2E_{|^1_1 X} - \delta, \tag{18}$$

where δ is the biexciton binding energy. Experimental results have shown that δ significantly varies depending on the nature and the size of the QD. The biexciton binding energy can therefore range from about 3 meV for InGaAs/GaAs QDs up to 27 meV for CdS/ZnS QDs [19]. Setting the laser frequency at half the biexciton energy, $2\hbar\omega_l = E_{|^2_2 X}$, and using the rotating wave approximation (RWA), the total Hamiltonian of the QD interacting with a linearly polarized laser pulse can be written as [14]

$$\mathcal{H}_S = \begin{pmatrix} \Delta & \Omega/2 & 0 \\ \Omega/2 & \delta/2 & \Omega/2 \\ 0 & \Omega/2 & -\Delta \end{pmatrix}, \tag{19}$$

where $\Delta = 2\alpha t$. In this Hamiltonian, the first, second, and third states represent the ground ($|0\rangle$), the singly excited ($|^1_1 X\rangle$), and the biexcitonic ($|^2_2 X\rangle$) states, respectively. The dipole moments of the two transitions $\langle 0|\mu|^1_1 X\rangle$ and $\langle ^1_1 X|\mu|^2_2 X\rangle$ were assumed to be identical. According to Eq. (6), only two relaxation operators model the ex-ph interactions: $\mathcal{S}_1 = |^1_1 X\rangle\langle ^1_1 X|$ and $\mathcal{S}_2 = 2|^2_2 X\rangle\langle ^2_2 X|$.

As seen in Eq. (12), the exciton-phonon interactions enter the description of the time-dependent dynamics via the spectral density $\mathcal{J}(\omega)$. With the small energy differences considered here, the interaction of the exciton with the acoustic phonon is dominant [8]. The phonon spectral density is therefore well approximated by the super-Ohmic distribution [47]:

$$\mathcal{J}(\omega) = \Lambda\omega^3 e^{-\omega^2/\omega_c^2}, \tag{20}$$

where Λ represents the exciton-phonon coupling constant and ω_c is the high-energy frequency cutoff. Previous estimations of the exciton-phonon interaction strength have shown that $\Lambda = 0.022$ ps^{-1} for GaAs QDs [11]. The frequency cutoff of the bath spectral density depends on the size of the QD. We set here $\omega_c = 0.72$ meV, which corresponds to a QD of 5 nm in diameter [48].

Using these parameters, we have calculated the final biexciton population, denoted $\mathcal{P}_f(^2_2 X)$, obtained for different values of the pulse area Θ and chirp parameter α. The results of these calculations are shown in Fig. 1. Different values of the biexciton binding energy were considered. A temperature of $T = 4$ K and an initial pulse duration of $\tau_0 = 2$ ps were set during the calculations. The results shown in Fig. 1 are almost identical to those reported by Glässl *et al.* [14], where a real-time path-integral approach was used to solve the excitonic dynamics [43]. However, discrepancies appear between our results and those reported in Ref. [14] for large values of the pulse area ($\Theta > 6\pi$) and small negative values of the chirp parameter $-20 < \alpha < 0$. These differences are due to the different ex-ph coupling strength and frequency cutoff of the phonon modes considered in both cases.

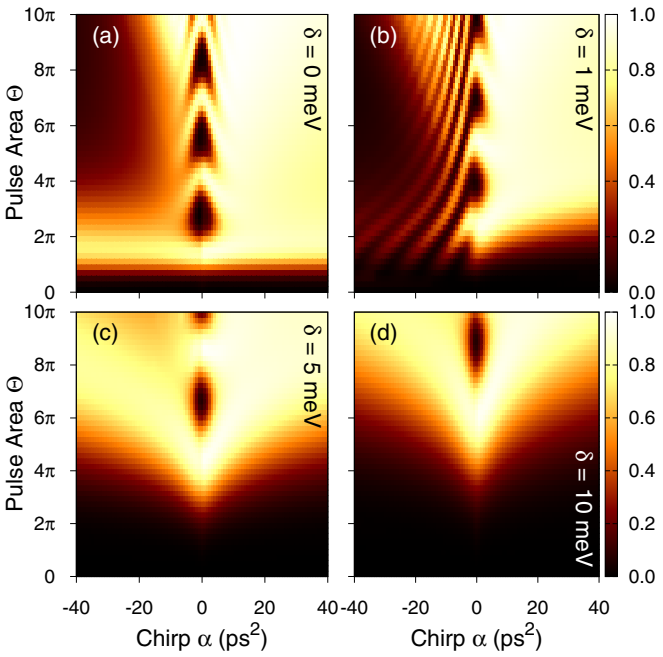

FIG. 1. (Color online) Variations of the final biexciton population with the pulse area (Θ) and chirp parameter (α) of the laser pulse for an isolated QD. Four different values of the biexciton binding energy δ are represented. A temperature of $T = 4$ K was set during the calculations.

As seen in Fig. 1, the pulse area threshold required to obtain an optimum biexciton generation increases with biexciton binding energy. In the ideal case in which $\delta = 0$, a pulse area of $\Theta_{\text{th}} = 2\pi$ is sufficient to obtain a optimum population on $|^2_2 X\rangle$. However, for $\delta = 10$ meV, this threshold increases to $\Theta_{\text{th}} = 10\pi$, which corresponds to a pulse 25 times more intense than for $\delta = 0$. Additionally, for $\delta = 10$ meV and $\Theta = 2\pi$, a negligible final biexciton population is obtained. This demonstrates the difficulty in obtaining an efficient biexciton generation using low-intensity pulses for quantum dots presenting a strong biexciton binding energy.

IV. BIEXCITON GENERATION IN COUPLED QUANTUM DOTS

To improve the biexciton generation for QDs presenting large values of δ, we study in this section the chirped pulse excitation of two neighboring QDs that are coupled with each other [22]. The two QDs are referred in the following as top (T) and bottom (B), and they are separated by a distance R. This distance can be precisely controlled by tuning the growth conditions of the dots [24], which is fixed to $R = 8.4$ nm in the following. Additionally, an external electric field, denoted F in the following, can be applied to the dimer of QDs when the latter is placed in an n-i Schottky

barrier [26,27]. This static external electric field can be used to shift the energy of selected excitonic states of the CQDs, which leads to a rich pattern of level anticrossings in its absorption spectrum [28].

We consider in the following all the 14 excited states of the CQDs up to two excitations. As in the preceding section, these states are labeled $|^{e_T e_B}_{h_T h_B} X\rangle$, where e_T (e_B) and h_T (h_B) are the number of excited electrons and holes in the top (bottom) QD, respectively. Our model consequently encompasses two localized excitons $|^{10}_{10}X\rangle$ and $|^{01}_{01}X\rangle$ and two indirect excitons $|^{10}_{01}X\rangle$ and $|^{01}_{10}X\rangle$. Similarly, several biexcitonic states are present in the model: two localized biexcitons $|^{20}_{20}X\rangle$ and $|^{02}_{02}X\rangle$, one segregated biexciton $|^{11}_{11}X\rangle$, two indirect biexcitons $|^{02}_{20}X\rangle$ and $|^{20}_{02}X\rangle$, and a set of trionic-like states, $|^{02}_{11}X\rangle$, $|^{20}_{11}X\rangle$, $|^{11}_{02}X\rangle$, and $|^{11}_{20}X\rangle$.

In the following, we aim to optimize the final biexciton population obtained on the top QD, i.e., the population of $|^{20}_{20}X\rangle$. The choice of the QD is of course arbitrary. We first present the model Hamiltonian describing the excitonic levels of the coupled QDs. We then explore the optical spectrum of the CQDs and study the efficiency of the biexciton generation obtained via ARP excitation.

A. Energy levels and mutual couplings in CQDs

An accurate determination of the exciton and biexciton energies of coupled InGaAs QDs has recently been derived from atomistic empirical pseudopotential calculations [49,50]. A description of these energies using a simple configuration-interaction approach can be found in the Appendix. Following the tight-binding parametrization developed in Ref. [49], we fix the excitation energy of the top QD to $E_{\,10}^{\,10}X = 1.587$ eV. The energy of the bottom QD can be precisely controlled experimentally by tuning its chemical or structural parameters [24,25,49]. As reported in Ref. [24], we consider a detuning of 10 meV between the two QDs and fix $E_{\,01}^{\,01}X = 1.597$ eV.

Due to the intrinsic charge-transfer character of the indirect excitons, the energies of $|^{10}_{01}X\rangle$ and $|^{01}_{10}X\rangle$ depend strongly on the value of the static electric field, F [31]. These energies are given by

$$E_{\,10}^{\,01}X(F) = E_{\,10}^{\,01,0}X - eFR, \tag{21}$$

$$E_{\,01}^{\,10}X(F) = E_{\,01}^{\,10,0}X + eFR. \tag{22}$$

Following [49], the zero-field energies of these indirect excitons were set to $E_{\,01}^{\,10,0}X = E_{\,10}^{\,01,0}X = 1.609$ eV [49]. As mentioned above, our model contains a total of nine biexcitonic states. The energies of the localized biexcitons, $|^{20}_{20}X\rangle$ and $|^{02}_{02}X\rangle$, are affected by the biexciton binding energy δ:

$$E_{\,20}^{\,20}X = 2E_{\,10}^{\,10}X - \delta, \tag{23}$$

$$E_{\,02}^{\,02}X = 2E_{\,01}^{\,01}X - \delta. \tag{24}$$

Following [50], the energy of the segregated biexciton, $|^{11}_{11}X\rangle$, is set to $E_{\,11}^{\,11}X = E_{\,10}^{\,10}X + E_{\,01}^{\,01}X + 6$ meV. Similarly to the indirect single excitons, the trion-like states experience a Stark shift induced by F. Their energies are, therefore, given by

$$E_{\,20}^{\,11}X(F) = E_{\,02}^{\,11,0}X - eFR, \tag{25}$$

$$E_{\,02}^{\,11}X(F) = E_{\,02}^{\,11,0}X + eFR, \tag{26}$$

$$E_{\,11}^{\,20}X(F) = E_{\,11}^{\,20,0}X + eFR, \tag{27}$$

$$E_{\,11}^{\,02}X(F) = E_{\,11}^{\,02,0}X - eFR. \tag{28}$$

As shown in the Appendix, the zero-field energies of these states are set here to $E_{\,20}^{\,11,0}X = E_{\,11}^{\,20,0}X = E_{\,20}^{\,20}X + 33$ meV and $E_{\,11}^{\,02,0}X(0) = E_{\,02}^{\,11,0}X = E_{\,02}^{\,02}X + 23$ meV. Finally, the energies of the indirect biexcitonic states are set to $E_{\,20}^{\,02}X = E_{\,02}^{\,20}X = E_{\,11}^{\,11}X + 74$ meV.

The excitonic and biexcitonic states described above interact with each other either via the electron or hole tunneling matrix elements, denoted t_e and t_h, respectively, or via a Förster excitonic coupling, denoted V_F [31,49]. The values of these different couplings depend strongly on the distance R between the two dots [49,51]. With a distance of $R = 8.4$ nm, the values of these couplings are set to $t_e = 5.1$ meV, $t_h = 0.4$ meV, and $V_F = 0.08$ meV [31,49]. The different couplings between the different excitons and biexcitons are straightforward to determine and are therefore not explicitly described here.

Due to these mutual interactions, the excitons and biexcitons formed delocalized excitonic and biexcitonic states. These noninteracting diagonal states are denoted $|X_n\rangle$ and $|B_m\rangle$, respectively, and they can be expressed as

$$|X_n\rangle = \sum_{ab,cd} \chi^{(n)}_{ab,cd} \left|^{ab}_{cd}X\right\rangle, \tag{29}$$

$$|B_m\rangle = \sum_{ab,cd} \beta^{(m)}_{ab,cd} \left|^{ab}_{cd}X\right\rangle. \tag{30}$$

Four of these states are of particular importance in the following. The states $|^{10}_{10}X\rangle$ and $|^{01}_{10}X\rangle$ are coupled by the tunneling matrix element t_e. Due to the strong value of t_e considered here, these two states can be mixed in two delocalized excitonic states, referred to as $|X_0\rangle$ and $|X_1\rangle$ in the following, if the energies $E_{\,10}^{\,10}X$ and $E_{\,10}^{\,01}X$ are brought in near resonance by the electric field. The states $|^{20}_{20}X\rangle$ and $|^{11}_{20}X\rangle$ interact also via t_e. Therefore, an important mixing of these two states in two delocalized biexcitonic states, denoted $|B_0\rangle$ and $|B_1\rangle$ in the following, can occur if the energies $E_{\,20}^{\,20}X$ and $E_{\,20}^{\,11}X$ are brought in near resonance by the electric field. As demonstrated in the following, the energetic variations of these four delocalized excitonic states induced by the axial electric field can be used to compensate for the effect of the biexciton binding energy.

B. Optical spectrum of the CQDs

The variation of the CQDs absorption spectrum with F is shown in Fig. 2. This absorption spectrum was calculated from

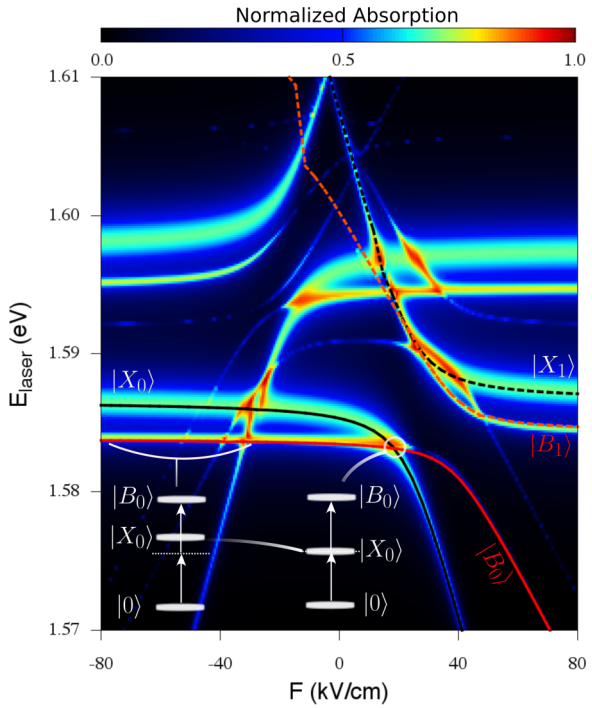

FIG. 2. (Color online) Variation of the CQD absorption spectrum with the laser frequency and the electric field. The energies of the diagonal excitonic states $|X_{0(1)}\rangle$ and $|B_{0(1)}\rangle$ are marked with black and red plain (dashed) lines, respectively.

the averaged ground-state population of the CQDs [52]:

$$A = 1 - \int_0^{t_\infty} dt |\langle 0|e^{-i\mathcal{H}_S t}|0\rangle|^2, \tag{31}$$

where $\mathcal{H}_S(t)$ refers to the Hamiltonian of the CQDs in interaction with a broad square laser pulse. The spectrum shown in Fig. 2 was calculated for $\delta = 5$ meV and continuous values of F ranging between ± 80 kV/cm. Each resonance observed in this figure corresponds to the excitation of a particular diagonal excitonic state $|X_n\rangle$ or biexcitonic state $|B_n\rangle$. The former case occurs when $\hbar\omega_l = E_{X_n}$. This is the case, for example, for the excitation of $|X_0\rangle$ and $|X_1\rangle$, which are marked by black plain and dashed lines, respectively, in Fig. 2. As seen in this figure, a level anticrossing between these two states appears for $F = 26.19$ kV/cm. The energies of $|X_0\rangle$ and $|X_1\rangle$, denoted E_{X_0} and E_{X_1}, are consequently shifted up and down when approaching the anticrossing. Due to the large value of t_e, E_{X_0} and E_{X_1} can be up to 10 meV below and above $E_{{}^{10}_{10}X}$ while remaining optically active.

The resonances induced by a two-photon excitation of a particular biexcitonic state, $|B_n\rangle$, occurs when $2\hbar\omega_l = E_{B_n}$. This is the case, for example, for the resonances marked by red plain and dashed lines in Fig. 2. These resonances correspond to the two-photon excitation of $|B_0\rangle$ and $|B_1\rangle$, respectively. As seen in Fig. 2, the energy of $|X_0\rangle$ is exactly half the energy of $|B_0\rangle$ for $F = 20.52$ kV/cm. Therefore, by setting the laser central frequency to $2\hbar\omega_l = E_{B_0}$, one obtains

$$E_{X_0} = E_{B_0} - E_{X_0} = \hbar\omega_l, \tag{32}$$

i.e., the central laser frequency is resonant with the $|0\rangle \rightarrow |X_0\rangle$ transition and also with the $|X_0\rangle \rightarrow |B_0\rangle$ transition. Let us stress once again that the diagonal biexciton state, $|B_0\rangle$, is not fully localized on $|{}^{20}_{20}X\rangle$ and is mixed (principally) with $|{}^{11}_{20}X\rangle$. However, for the values of F reported in the following, a negligible mixing between these two states is obtained and $|B_0\rangle$ is localized at more that 80% on $|{}^{20}_{20}X\rangle$, i.e., $|\beta^{(0)}_{20,20}| > 0.90$ in Eq. (30).

C. ARP excitation of CQDs

The total Hamiltonian of the CQDs in interaction with the laser pulse can be written as

$$\begin{aligned}\mathcal{H}_S = &\sum_{n=1,4} (\xi_{X_n} - \Delta)|X_n\rangle\langle X_n| \\ &+ \sum_{m=1,9} (\xi_{B_m} - 2\Delta)|B_m\rangle\langle B_m| \\ &+ \sum_{n=1,4} (\Omega_{X_n,0}|X_n\rangle\langle 0| + \text{H.c}) \\ &+ \sum_{m=1,9}\sum_{n=1,4} \left(\Omega_{B_m,X_n}|B_m\rangle\langle X_n| + \text{H.c}\right)\end{aligned} \tag{33}$$

with $\Delta = 2\alpha t$ and where $\Omega_{X,Y}$ is the laser-induced coupling between the states X and Y of the CQDs. In Eq. (33), $\xi_{X_n} = E_{X_n} - \hbar\omega_l$ and $\xi_{B_n} = E_{B_n} - 2\hbar\omega_l$ are the detuning between the central laser frequency and the diagonal excitonic and biexcitonic energies, respectively.

According to Eq. (6), there are a total of 13 relaxation operators here modeling the ex-ph interactions. These operators are defined in the local basis by

$$\mathcal{S}_{abcd} = \sum_{ab,cd} \eta_{ab,cd} \left|{}^{ab}_{cd}X\right\rangle\left\langle{}^{ab}_{cd}X\right|, \tag{34}$$

where $\eta_{ab,cd}$ is the number of excitons in the state $|{}^{ab}_{cd}X\rangle$. We therefore assume that all the excitons (biexcitons) interact with the same strength with the phonon modes regardless of the location of the electron(s) and hole(s) in the CQDs. An evaluation of these different ex-ph couplings could be performed using the deformation and piezoelectric fields of the material considered. These delicate calculations are, however, outside the scope of this paper.

This approximation is motivated here by the difficulty to precisely determine the relative ex-ph coupling strength for all the different states.

The Hamiltonian described above was used to simulate the excitation of CQDs by a chirped laser pulse and extract the final biexciton population on $|B_0\rangle$. The variations of this final biexciton population, denoted $\mathcal{P}_f(B_0)$, with the pulse area Θ and the chirp parameter α are shown in Fig. 3. Four different cases are presented, each one corresponding to a given combination of values for δ and F that leads to $2E_{X_0} = E_{B_0}$. A temperature of $T = 4$ K was set during the calculations with a pulse duration of $\tau_0 = 2$ ps. We limit the analysis to values of α ranging between ± 20 ps^{-2}. As seen in Fig. 3, the resulting variations of the final biexciton population are very similar to those obtained for an isolated quantum dot with $\delta = 0$ [see Fig. 1(a)]. In each case, an optimum population transfer to $|B_0\rangle$ is obtained for $\alpha = 20$ ps^2 with a threshold pulse area of only $\Theta_{\text{th}} \simeq 2\pi$.

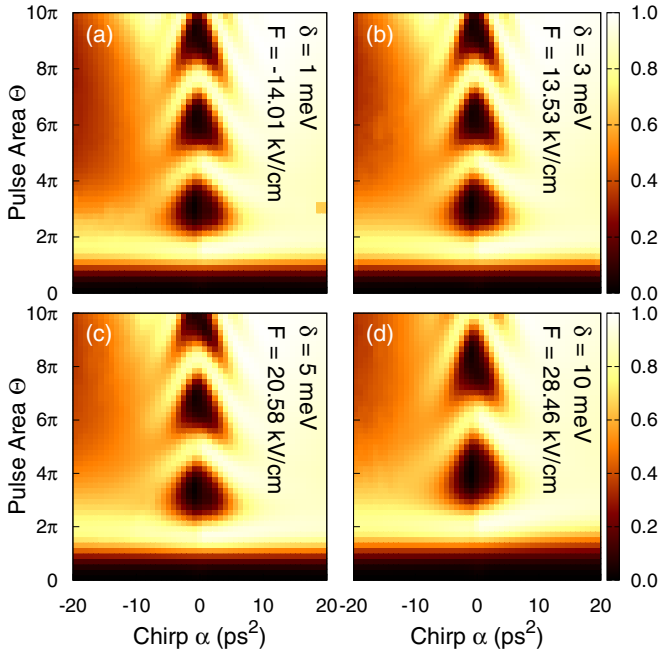

FIG. 3. (Color online) Variations of the final biexciton population on $|B_0\rangle$ with the pulse area and the chirp parameter. Four different combinations of values for δ and F are represented. A temperature of $T = 4$ K and an initial pulse duration $\tau_0 = 2$ ps were used during the calculations.

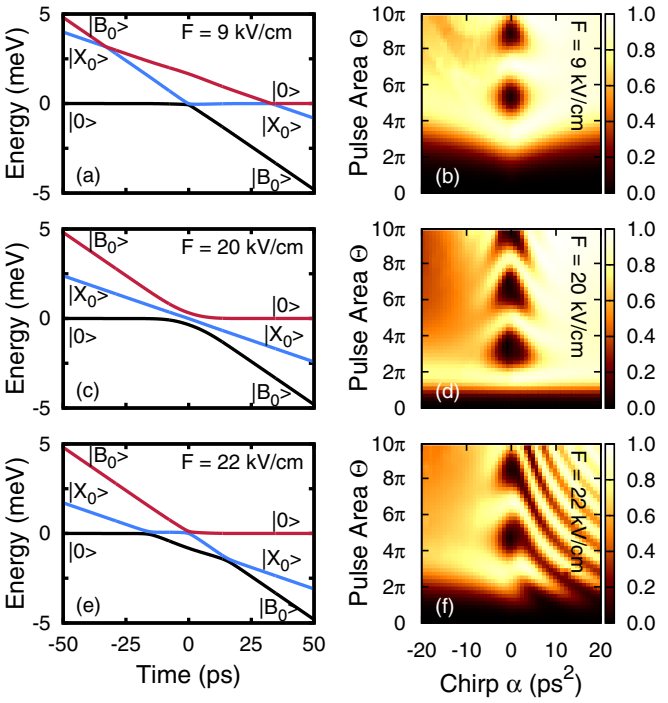

FIG. 4. (Color online) Time evolution of the relevant dressed state energies for a CQD with $\delta = 5$ meV, $\Theta = 2\pi$, and $\alpha = 20$ ps^2. The evolution for $\alpha = -20$ ps^2 can be read from the plots by reversing the time axis. The corresponding biexciton generation maps are shown in the right column.

The results shown in Fig. 3 demonstrate the possibility to optimize the biexciton generation in the top QD by engineering the interactions between the two dots. This cooperative effect between the two QDs leads to a significant improvement of biexciton generation when using a low-intensity laser pulse in materials presenting an important biexciton binding energy. However, the maximum value of δ that can be compensated is intrinsically limited by the magnitude of the electronic coupling t_e with $\delta_{\max} \simeq 2t_e$.

The time evolution of the dressed states energies obtained for $\delta = 5$ meV, $\Theta = 2\pi$, and $\alpha = 20$ ps^{-2} are represented for different values of F in Fig. 4. The right column shows the corresponding variations of the biexciton generation with Θ and α. As already explained above, an optimum biexciton generation is obtained for $\delta = 5$ meV and $F = 20.52$ kV/cm. The corresponding time evolution of the dressed state energies is shown in Fig. 4(c). Long before and after the pulse, it is possible to identify the dressed states with the ground state $|0\rangle$, the diagonal singly excited state $|X_0\rangle$, and the final biexcitonic state $|B_0\rangle$. The other dressed states have energies that are far above those three and have therefore a negligible impact on the dynamics. For $F = 20.52$ kV/cm, a single anticrossing between the relevant dressed states is obtained at $t = 0$. The splitting of this central anticrossing is large enough, even for $\Theta = 2\pi$, to ensure the adiabaticity of the dynamics and therefore to enable a robust biexciton generation. The asymmetry observed in Fig. 4(d) between positive and negative values of α is due to the different dressed states adiabatically followed during the dynamics [14]. For $\alpha > 0$, the dynamics follows the lowest dressed state and is therefore not strongly perturbed by the ex-ph interactions. On the contrary, for $\alpha < 0$ the dynamics follows the highest dressed state and is therefore more sensitive to phonon-induced dephasing [14].

As seen in Figs. 4(a) and 4(e), modifying the value of F principally shifts the energy of $|X_0\rangle$ and results in the creation of multiple anticrossings between the different dressed states. These anticrossings are too narrow for the adiabaticity condition to be respected, which lessens the quality of the biexciton generation. As a consequence, the pulse area threshold required to obtain an optimum biexciton generation increases.

To evaluate the stability of the effect described above, we have calculated the variations of $\mathcal{P}_f(B_0)$ for values of F ranging between 0 and 40 kV/cm. The results of these calculations are shown in Fig. 5. All the calculations were performed with $\delta = 5$ meV, $T = 4$ K, and for different values of Θ. In each case, a value of $F = 20.52$ kV/cm significantly improves the biexciton generation. This improvement of the biexciton generation is stable toward small fluctuations of the external electric field as a final biexciton population superior to 0.8 is obtained for values of F ranging between 20 and 22 kV/cm.

As seen in Fig. 5, a value of the electric field of $F = 31$ kV/cm completely inhibits the biexciton generation even for large values of Θ. This total cancellation of the biexciton generation is due to destructive quantum interference between the different optical pathways available between the ground state and final biexciton state. The signature of such interference has been observed in a broad range of situations, such as the electronic transmission of molecular junctions [53,54]

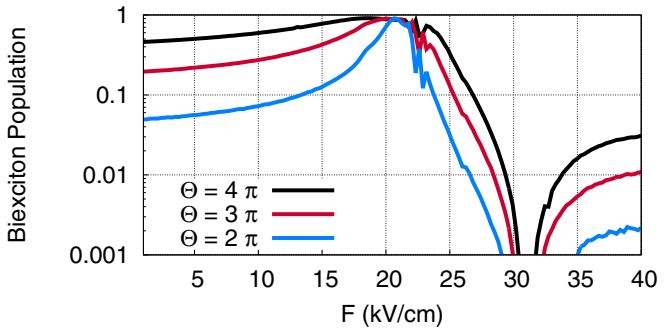

FIG. 5. (Color online) Variations of the final population of $|B_0\rangle$ for $\alpha = 20\ \text{ps}^2$, $\delta = 5$ meV, $T = 4$ K, and different values of the pulse area.

and quantum dots [55], the fission of singlet excited states in molecular crystals [56], or the charge propagation through organic molecules [57,58]. In the CQDs studied here, the four diagonal excitonic states, $|X_m\rangle$, act as intermediate states during the excitation of the CQD from its ground state to the biexcitonic state $|B_0\rangle$. In the limit where all the excitonic states are off-resonant with the central laser frequency, destructive interference between the different pathways is obtained when [53,54] $\sum_{n=1}^{4} \xi_{X_n}^{-1} \langle 0|\mu|X_n\rangle\langle X_n|\mu|B_0\rangle = 0$. As can be seen in Fig. 5, the biexciton generation can be switched ON or OFF, with a large ON/OFF ratio, by simply tuning the value of the electric field.

Finally, Fig. 6 shows the effect of the temperature on the biexciton generation for the CQDs and the isolated QD. In both cases, a biexciton binding energy of $\delta = 5$ meV was considered. The value of the electric field along the CQDs was tuned to $F = 20.52$ kV/cm to obtain an optimum biexciton generation. As seen in Fig. 6, the efficiency of the biexciton generation decreases with the temperature. Hence, if a nearly optimal biexciton generation is obtained in the CQDs for $\Theta = 2\pi$ at $T = 4$ K, at $T = 20$ K the final biexciton population reaches only 0.6 and drops to 0.4 at $T = 80$ K. Figure 6 also reveals that that biexciton population behaves nonmonotonically with the pulse area. For values of $\Theta > 2\pi$, the biexciton population initially decreases, only to increase again after $\Theta = 4\pi$. Similar variations of the final biexciton population have been reported for isolated QDs [14], and they are due to the resonance character of the ex-ph coupling [59]. Consequently, the increase and decrease of the final biexciton population depend strongly on the interplay between the phonon spectral density and the envelope of the laser pulse.

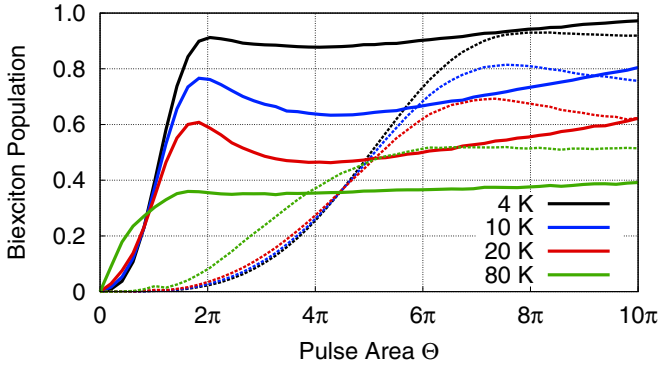

FIG. 6. (Color online) Temperature dependence of the biexciton generation depending on the pulse area for $\alpha = 20\ \text{ps}^2$ and $\delta = 5$ meV. Two cases are reported: the CQDs with $F = 20.52$ kV/cm (plain lines) and the isolated QD (dashed lines).

Figure 6 also shows the impact of temperature on the biexciton generation in a single quantum dot with $\delta = 5$ meV. As mentioned above, the threshold pulse area needed to obtain a maximum biexciton population is much larger here than for the CQDs. Hence a pulse area of $\Theta = 8\pi$ is required to obtain a maximum biexciton generation. Note, however, that for $T = 80$ K, the final biexciton population saturates at 0.5. Consequently, at high temperature and large pulse area, the biexciton generation is more efficient in an isolated QD than in CQDs, as only one single excited states is then involved in the excitonic dynamics.

V. CONCLUSION

In this paper, we presented numerical results of the chirped pulse excitation of an isolated quantum dot and a quantum dot dimer. These simulations were based on a non-Markovian quantum jump approach to account for the charge-phonon interactions combined with a Chebyshev expansion of the evolution operator. The results obtained with this numerical approach on isolated quantum dots are in good agreement with previously reported results. As already reported in the literature, the efficiency of the biexciton generation decreases significantly with the biexciton binding energy. Consequently, intense laser pulses are required to obtain an efficient biexciton generation in isolated quantum dots presenting a biexciton binding energy of a few meV.

We have then studied the excitation of two coupled QDs placed in an external static electric field and excited by a chirped laser pulse. The absorption spectrum of this system reveals the presence of different level anticrossings resulting from the mixing of its excitonic and biexcitonic states. We have demonstrated here that the value of the electric field can be tuned to compensate for the effect of the biexciton binding energy during the ARP excitation of the CQDs. Consequently, for well-defined values of the electric field, a resonant two-photon absorption to a diagonal biexcitonic state can be obtained. Our results show that the excitation obtained in this situation is similar to the one obtained for an isolated QD with a null biexciton binding energy. Hence a very efficient biexciton generation can be obtained using low-intensity pulses even for biexciton binding energies of a few tens of meV.

Our calculations have also demonstrated the possibility to tune the electric field in order to obtain destructive quantum interference during the chirped pulse excitation of the CQDs. When such interference occurs, the biexciton generation is totally inhibited and the final biexciton generation drops to zero even for large values of the pulse area. As a consequence, the biexciton generation can be easily turned ON or OFF by precisely tuning the value of the electric field along the CQDs. The large ON/OFF ratio obtained with this approach might be important for a future experimental verification of the results presented here. While it represents a significant

TABLE I. Single-particle electron and hole energies and Coulomb integrals used to evaluate the exciton and biexciton energies of the CQDs.

ϵ_e^T	1.458 eV	ϵ_h^T	−0.156 eV
ϵ_e^B	1.463 eV	ϵ_h^B	−0.161 eV
J_{eh}	27 meV	$J_{eh}^{\times}$	10 meV
J_{hh}	31 meV	$J_{hh}^{\times}$	14 meV
J_{ee}	29 meV	$J_{ee}^{\times}$	12 meV

experimental challenge, the utilization of chirped laser pulses on CQDs provides a unique solution to probe and control the optoelectronic properties of complex multilevel quantum systems.

APPENDIX: CONFIGURATION INTERACTION ENERGIES OF THE EXCITON AND BIEXCITON STATES

Following Refs. [49,50], we express the energy of the different biexciton states as a configuration expansion including the single-particle energies of electrons, $\epsilon_e^{T/B}$, and holes, $\epsilon_h^{T/B}$, on the top (T) and bottom (B) quantum dot, and the different Coulomb integrals. The energy of the localized excitons reads

$$E^{10}_{10} = \epsilon_e^T - \epsilon_h^T - J_{eh},$$
$$E^{01}_{01} = \epsilon_e^B - \epsilon_h^B - J_{eh},$$

where J_{eh} is the Coulomb integral between an electron and a hole localized on the same QD. We assign here a positive value to all the Coulomb integrals and adjust their respective signs in the CI expansion. We also assume that all the Coulomb integrals in the top and bottom QD are identical. The zero-field energy of the indirect excitons reads

$$E^0_{\substack{01\\10}} = \epsilon_e^B - \epsilon_h^T - J_{eh}^{\times},$$
$$E^0_{\substack{10\\01}} = \epsilon_e^T - \epsilon_h^B - J_{eh}^{\times},$$

where $J_{eh}^{\times}$ is the Coulomb integral between an electron and a hole localized on two different QDs. The energy of the segregated biexciton state is given by

$$E^{11}_{11} = E^{10}_{10} + E^{01}_{01} + J_{ee}^{\times} + J_{hh}^{\times} - 2J_{eh}^{\times},$$

where $J_{ee\,(hh)}^{\times}$ is the Coulomb integral between two electrons (holes) localized on two different QDs. Similarly, $J_{eh}^{\times}$ is the electron-hole Coulomb integral between an electron and a hole localized on two different QDs. The zero-field energies of the trion-like states are given by

$$E^0_{\substack{11\\20}} = E^{10}_{10} + E^0_{\substack{01\\10}} - J_{eh} - J_{eh}^{\times} + J_{ee}^{\times} + J_{hh},$$
$$E^0_{\substack{11\\02}} = E^{01}_{01} + E^0_{\substack{10\\01}} - J_{eh} - J_{eh}^{\times} + J_{ee}^{\times} + J_{hh},$$
$$E^0_{\substack{20\\11}} = E^{10}_{10} + E^0_{\substack{10\\01}} - J_{eh} - J_{eh}^{\times} + J_{ee} + J_{hh}^{\times},$$
$$E^0_{\substack{02\\11}} = E^{01}_{01} + E^0_{\substack{01\\10}} - J_{eh} - J_{eh}^{\times} + J_{ee} + J_{hh}^{\times},$$

where $J_{ee\,(hh)}$ is the Coulomb integrals between two electrons (holes) localized on the same QDs. Finally the energies of the delocalized biexciton states are given by

$$E^0_{\substack{02\\20}} = 2E^0_{\substack{01\\10}} - 2J_{eh}^{\times} + J_{ee} + J_{hh},$$
$$E^0_{\substack{20\\02}} = 2E^0_{\substack{10\\01}} - 2J_{eh}^{\times} + J_{ee} + J_{hh},$$

following Refs. [49,50] and assuming a static detuning of 10 meV between the excitation energies of the two QDs. This detuning that originates here is a 5 meV shift of the single-particle electron and hole energy between the top and bottom QD. All the parameters used to evaluate the excitonic and biexciton energies are given in Table I.

[1] E. Moreau, I. Robert, L. Manin, V. Thierry-Mieg, J. M. Gérard, and I. Abram, Phys. Rev. Lett. **87**, 183601 (2001).

[2] R. M. Stevenson, R. J. Young, P. Atkinson, K. Cooper, D. A. Ritchie, and A. J. Shields, Nature (London) **439**, 179 (2006).

[3] A. Zrenner, E. Beham, S. Stufler, F. Findeis, M. Bichler, and G. Abstreiter, Nature (London) **418**, 612 (2002).

[4] A. J. Ramsay, A. Venu Gopal, E. M. Gauger, A. Nazir, B. W. Lovett, A. M. Fox, and M. S. Skolnick, Phys. Rev. Lett. **104**, 017402 (2010).

[5] A. J. Ramsay, T. M. Godden, S. J. Boyle, E. M. Gauger, A. Nazir, B. W. Lovett, A. M. Fox, and M. S. Skolnick, Phys. Rev. Lett. **105**, 177402 (2010).

[6] N. V. Vitanov, T. Halfmann, B. W. Shore, and K. Bergmann, Annu. Rev. Phys. Chem. **52**, 773 (2001).

[7] S. Lüker, K. Gawarecki, D. E. Reiter, A. Grodecka-Grad, V. M. Axt, P. Machnikowski, and T. Kuhn, Phys. Rev. B **85**, 121302 (2012).

[8] A. Debnath, C. Meier, B. Chatel, and T. Amand, Phys. Rev. B **86**, 161304 (2012).

[9] P. R. Eastham, A. O. Spracklen, and J. Keeling, Phys. Rev. B **87**, 195306 (2013).

[10] S. Guerin, S. Thomas, and H. R. Jauslin, Phys. Rev. A **65**, 023409 (2002).

[11] Y. Wu, I. M. Piper, M. Ediger, P. Brereton, E. R. Schmidgall, P. R. Eastham, M. Hugues, M. Hopkinson, and R. T. Phillips, Phys. Rev. Lett. **106**, 067401 (2011).

[12] C.-M. Simon, T. Belhadj, B. Chatel, T. Amand, P. Renucci, A. Lemaitre, O. Krebs, P. A. Dalgarno, R. J. Warburton, X. Marie, and B. Urbaszek, Phys. Rev. Lett. **106**, 166801 (2011).

[13] A. Debnath, C. Meier, B. Chatel, and T. Amand, Phys. Rev. B **88**, 201305 (2013).

[14] M. Glässl, A. M. Barth, K. Gawarecki, P. Machnikowski, M. D. Croitoru, S. Lüker, D. E. Reiter, T. Kuhn, and V. M. Axt, Phys. Rev. B **87**, 085303 (2013).

[15] K. Gawarecki, S. Luker, D. E. Reiter, T. Kuhn, M. Glassl, V. M. Axt, A. Grodecka-Grad, and P. Machnikowski, Phys. Rev. B **86**, 235301 (2012).

[16] M. Glässl, A. M. Barth, and V. M. Axt, Phys. Rev. Lett. **110**, 147401 (2013).

[17] R. M. Stevenson, R. J. Young, P. Atkinson, K. Cooper, D. A. Ritchie, and A. J. Shields, Nature (London) **439**, 179 (2006).

[18] Y. Léger, L. Besombes, L. Maingault, and H. Mariette, Phys. Rev. B **76**, 045331 (2007).
[19] U. Woggon, K. Hild, F. Gindele, W. Langbein, M. Hetterich, M. Grun, and C. Klingshirn, Phys. Rev. B **61**, 12632 (2000).
[20] C. Creatore, R. T. Brierley, R. T. Phillips, P. B. Littlewood, and P. R. Eastham, Phys. Rev. B **86**, 155442 (2012).
[21] R. T. Brierley, C. Creatore, P. B. Littlewood, and P. R. Eastham, Phys. Rev. Lett. **109**, 043002 (2012).
[22] N. N. Ledentsov, V. A. Shchukin, M. Grundmann, N. Kirstaedter, J. Böhrer, O. Schmidt, D. Bimberg, V. M. Ustinov, A. Y. Egorov, A. E. Zhukov, P. S. Kop'ev, S. V. Zaitsev, N. Y. Gordeev, Z. I. Alferov, A. I. Borovkov, A. O. Kosogov, S. S. Ruvimov, P. Werner, U. Gösele, and J. Heydenreich, Phys. Rev. B **54**, 8743 (1996).
[23] Z. R. Wasilewski, S. Fafard, and J. P. McCaffrey, J. Cryst. Growth **201-202**, 1131 (1999).
[24] B. D. Gerardot, I. Shtrichman, D. Hebert, and P. M. Petroff, J. Cryst. Growth **252**, 44 (2003).
[25] J. M. Garcia, T. Mankad, P. O. Holtz, P. J. Wellman, and P. M. Petroff, Appl. Phys. Lett. **72**, 44 (1998).
[26] J. Peng, C. Hermannstädter, M. Witzany, M. Heldmaier, L. Wang, S. Kiravittaya, A. Rastelli, O. G. Schmidt, P. Michler, and G. Bester, Phys. Rev. B **81**, 205315 (2010).
[27] G. J. Beirne, C. Hermannstädter, L. Wang, A. Rastelli, O. G. Schmidt, and P. Michler, Phys. Rev. Lett. **96**, 137401 (2006).
[28] M. Scheibner, M. Yakes, I. V. Bracker, A. S. Ponomarev, M. F. Doty, C. S. Hellberg, L. J. Whitman, T. L. Reinecke, and D. Gammon, Nat. Phys. **4**, 291 (2008).
[29] E. A. Stinaff, M. Scheibner, A. S. Bracker, I. V. Ponomarev, V. L. Korenev, M. E. Ware, M. F. Doty, T. L. Reinecke, and D. Gammon, Science **311**, 636 (2006).
[30] B. Szafran, T. Chwiej, F. M. Peeters, S. Bednarek, J. Adamowski, and B. Partoens, Phys. Rev. B **71**, 205316 (2005).
[31] J. E. Rolon and S. E. Ulloa, Phys. Rev. B **79**, 245309 (2009).
[32] L. Quiroga and N. F. Johnson, Phys. Rev. Lett. **83**, 2270 (1999).
[33] M. Bayer, P. Hawrylak, K. Hinzer, S. Fafard, M. Korkusinski, Z. R. Wasilewski, O. Stern, and A. Forchel, Science **291**, 451 (2001).
[34] L. Robledo, J. Elzerman, G. Jundt, M. Atatüre, A. Högele, S. Fält, and A. Imamoglu, Science **320**, 772 (2008).
[35] C. Meier and D. J. Tannor, J. Chem. Phys. **111**, 3365 (1999).
[36] D. P. S. McCutcheon, N. S. Dattani, E. M. Gauger, B. W. Lovett, and A. Nazir, Phys. Rev. B **84**, 081305 (2011).
[37] M. Glässl, A. Vagov, S. Lüker, D. E. Reiter, M. D. Croitoru, P. Machnikowski, V. M. Axt, and T. Kuhn, Phys. Rev. B **84**, 195311 (2011).
[38] J. Piilo, S. Maniscalco, K. Härkönen, and K.-A. Suominen, Phys. Rev. Lett. **100**, 180402 (2008).
[39] H. Tal-Ezer and R. Kosloff, J. Chem. Phys. **80**, 3967 (1984).
[40] K. Mølmer, Y. Castin, and J. Dalibard, J. Opt. Soc. Am. B **10**, 524 (1993).
[41] J. Piilo, K. Härkönen, S. Maniscalco, and K.-A. Suominen, Phys. Rev. A **79**, 062112 (2009).
[42] P. Rebentrost, R. Chakraborty, and A. Aspuru-Guzik, J. Chem. Phys. **131**, 184102 (2009).
[43] A. Vagov, M. D. Croitoru, M. Glässl, V. M. Axt, and T. Kuhn, Phys. Rev. B **83**, 094303 (2011).
[44] H.-P. Beuer and F. Petruccione, *The Theory of Open Quantum Systems* (Oxford University Press, Oxford, 2002).
[45] M. Ndong, H. Tal-Ezer, R. Kosloff, and C. P. Koch, J. Chem. Phys. **132**, 064105 (2010).
[46] H. Tal-Ezer, R. Kosloff, and I. Schaefer, J. Sci. Comput. **53**, 211 (2012).
[47] U. Weiss, *Quantum Dissipative Dynamics* (World Scientific, Singapore, 1993).
[48] A. V. Fedorov, A. V. Baranov, and K. Inoue, Phys. Rev. B **56**, 7491 (1997).
[49] G. Bester, A. Zunger, and J. Shumway, Phys. Rev. B **71**, 075325 (2005).
[50] J. Peng and G. Bester, Phys. Rev. B **82**, 235314 (2010).
[51] A. S. Bracker, M. Scheibner, M. F. Doty, E. A. Stinaff, I. V. Ponomarev, J. C. Kim, L. J. Whitman, T. L. Reinecke, and D. Gammon, Appl. Phys. Lett. **89** 233110 (2006).
[52] Following [31], the absorbtion spectrum is calculated via the average ground-state population: $A = (1/t_\infty)\int_0^\infty dt\,|\langle 0|\exp(-i\frac{\mathcal{H}}{\hbar}t)|0\rangle|^2$, where t_∞ is set to be long enough to capture several amplitude oscillations of the time-dependent dynamics. To simulate the continuous excitation of the system by a broad square laser pulse, $\Omega(t)$ is set to $\Omega(t) = \Omega_0 \exp(-i\omega_l t)$ with the pulse amplitude set to $\Omega_0 = 10\mu$eV in our calculations.
[53] N. Renaud, M. A. Ratner, and C. Joachim, J. Chem. Phys. B **115**, 5582 (2011).
[54] P. Sautet and C. Joachim, Chem. Phys. Lett. **153**, 511 (1988).
[55] Y. Han, W.-J. Gong, H.-M. Wang, and A. Du, J. Appl. Phys. **112**, 123701 (2012).
[56] F. Mirjani, N. Renaud, N. Gorczak, and F. C. Grozema, J. Phys. Chem. C **118**, 14192 (2014).
[57] C. Patoux, C. Coudret, J.-P. Launay, C. Joachim, and A. Gourdon, Inorg. Chem. **36**, 5037 (1997).
[58] N. Renaud, D. Powell, M. Zarea, B. Movaghar, M. R. Wasielewski, and M. A. Ratner, J. Phys. Chem. A **117**, 5899 (2013).
[59] P. Machnikowski and L. Jacak, Phys. Rev. B **69**, 193302 (2004).